Materials & Design 221 (2022) 110948

Contents lists available at ScienceDirect

Materials & Design

journal homepage: www.elsevier.com/locate/matdes

Quantification of room temperature strengthening of laser shock peened Ni-based superalloy using synchrotron microdiffraction

Guangni Zhou [a,b], Yubin Zhang [b,*], Wolfgang Pantleon [b], Jiawei Kou [a], Upadrasta Ramamurty [c], Xipeng Tan [d], Sihai Luo [e], Weifeng He [e], Ching-Shun Ku [f], Ching-Yu Chiang [f], Nobumichi Tamura [g], Kai Chen [a,*]

[a] Center for Advancing Materials Performance from the Nanoscale (CAMP-Nano), State Key Laboratory for Mechanical Behavior of Materials, Xi'an Jiaotong University, Xi'an, Shaanxi 710049, PR China
[b] Department of Civil and Mechanical Engineering, Technical University of Denmark, Kongens Lyngby 2800, Denmark
[c] School of Mechanical and Aerospace Engineering, Nanyang Technological University, Singapore 639798, Singapore
[d] Department of Mechanical Engineering, National University of Singapore, 9 Engineering Drive 1, Singapore 117575, Singapore
[e] Science and Technology on Plasma Dynamics Laboratory, Air Force Engineering University, Xi'an 710038, PR China
[f] National Synchrotron Radiation Research Center, Hsinchu 30076, Taiwan, ROC
[g] Advanced Light Source, Lawrence Berkeley National Laboratory, CA 94720, USA

HIGHLIGHTS

- Redundant dislocations are revealed to play a dominant role in laser shock peening induced plastic deformation in Ni-based superalloys.
- Local dislocation densities in γ and γ′ phases are quantified separately using μXRD in a laser shock peened Ni-based superalloy.
- A quantitative relationship between micro-scale local hardness increment and dislocation density is established over a millimeter range.

GRAPHICAL ABSTRACT

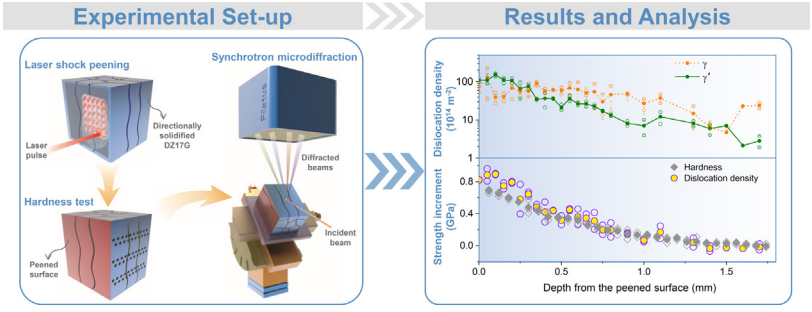

ARTICLE INFO

Article history:
Received 2 May 2022
Revised 23 June 2022
Accepted 11 July 2022
Available online 14 July 2022

Keywords:
Hardening
Dislocation density
Laser treatment
Ni-based superalloys
Synchrotron diffraction

ABSTRACT

Laser shock peening (LSP), a surface modification technique, is promising to enhance the strength and wear resistance for Ni-based superalloys. To understand the strengthening mechanism in a laser shock peened Ni-based superalloy DZ417G, we utilize synchrotron poly- and monochromatic X-ray microdiffraction, as well as electron microscopy and microhardness to quantify the local microstructures and mechanical properties at various depths. In the 1.2-mm-deep hardened layer, the microhardness increases monotonically by ~50% from the unaffected interior to the surface. Quantitative microdiffraction analysis shows that large amounts of dislocations are introduced by LSP. High densities of 7.1×10^{15} m^{-2} and 11.8×10^{15} m^{-2} are seen close to the peened surface for the γ- and γ′-phases, respectively, which are 5 and 20 times of those in the unaffected region. Different gradients of dislocation density are observed for the two phases from interior to surface, and their combined effect accounts well for the hardness increment. Due to the unaltered γ′-precipitates and chemical composition in the LSP affected zone, the large density of dislocations dominates the observed strengthening. Combined poly- and monochromatic X-ray microdiffraction allows quantifying the local microstructures of plastic deformation over a large sampling scale that can hardly be achieved using other materials characterization techniques.

* Corresponding authors.
E-mail addresses: yubz@mek.dtu.dk (Y. Zhang), kchenlbl@gmail.com (K. Chen).

https://doi.org/10.1016/j.matdes.2022.110948
0264-1275/

1. Introduction

Ni-based superalloys possess exceptional combination of high-temperature strength, toughness, as well as corrosion and oxidation resistance. They are ideal for manufacturing gas turbine blades and bladed disks (blisks) of aeronautic and astronautic engines, which are exposed to extreme environments in service [1,2]. The superior properties of these superalloys are mainly due to the precipitation strengthening provided by the cuboidal-shaped γ′-particles and the solid solution strengthening of the γ-matrix [3]. Fretting fatigue damage occurring in the connecting structures between blades and disk such as dovetail attachments is one of the major sources of failure in gas turbine engines [4,5]. Surface mechanical treatments by processes such as shot peening and laser shock peening (LSP) are thus necessary to strengthen such components [6,7]. During LSP, a high-power laser pulse ablates a protective overlay (tape, paint, or aluminium foil) into plasma. A transparent overlay (e.g., glass or water) is typically used to confine the generated plasma, such that shock waves with peak pressures of the order of several GPa can be produced. As the shock waves propagate into the interior of the samples, the peened materials experience severe plastic deformation at an ultrahigh strain rate (10^6 s^{-1} or higher), resulting in significant hardening [8]. A particular advantage of LSP over shot peening is its ability to induce a hardened layer (termed 'case') substantially deeper into the material below the peened surfaces. Case depths of more than 1 mm can be achieved using LSP, causing, at the same time, a much smaller surface roughness than shot peening [9]. These two factors improve fatigue strength, friction and fretting wear resistances greatly [10–15].

For the Ni-based superalloys, LSP has been shown to increase room-temperature tensile strength and vibrational fatigue strength by 25–33% and 169%, respectively [14,15], and introduce compressive residual stresses up to 600 MPa near the surface [16]. Moreover, even after annealing for 10 h at 900 °C, which is a higher temperature than the typical service temperature of dovetail joints of turbine engines, the beneficial effects brought about by LSP are still effective without significant relief [17]. All these advantages make LSP a promising technique for extending the lifetime of Ni-based superalloy blades.

While LSP is already deployed in certain industrial fields that utilize Ni-based superalloy and other alloys, certain crucial problems related to the strengthening mechanisms involved require further in-depth understanding. Transmission electron microscopy (TEM) investigation has revealed that high densities of dislocations are produced by the severe plastic deformation during LSP, which, sometimes, leads to microstructural refinement [18–23]. A detailed quantitative analysis that assesses the potential contributions from dislocations and microstructural refinement to the overall enhancement in strength is yet to be performed. LSP produces a deformed layer in the millimeter range with decreasing plastic strain from the surface to the interior. The correlation between the local microstructure and the local strength has not been established yet, because the high dislocation density produced by LSP is scarcely possible to measure using TEM, in which the micron-scale viewing range is only one-thousandth of the thickness of the case, hence an unrealistically large number of specimens would be necessary to cover the entire case (as obvious from [22]). More importantly, it has not yet been attempted to establish a direct evidence for microstructural differences between γ and γ′ phases after severe plastic deformation at the ultrahigh strain rate induced by LSP, for example the local dislocation density. It is important to quantify the contributions of the different strengthening mechanisms from each phase locally in the laser shock peened Ni-based superalloys. All these issues demand a novel investigation method that allows a quantitative measurement of both, the local mechanical strength and the local dislocation density in γ and γ′ phases while covering the whole depth of the peened case.

In this paper, we utilize the advanced scanning synchrotron micro X-ray diffraction (μXRD) [24] to study the gradient microstructure in a directionally solidified Ni-based superalloy after LSP. With a micro-sized high-intensity X-ray beam and a high-precision scanning stage, the local microstructure is readily mapped to cover a millimetre-sized area from the peened surface to the interior with spatial resolution on the scale of micrometers. By combining polychromatic and monochromatic X-ray diffraction signals [25], the local dislocation content in each individual microstructural phase, γ and γ′, is quantified. Such a quantitative analysis provides key insights for understanding the effects of LSP and for revealing the strengthening mechanisms of laser shock peened Ni-based superalloys.

2. Materials and experiments

2.1. Materials and LSP treatment

A directionally solidified Ni-based superalloy DZ417G is investigated. The nominal composition of the alloy is listed in Table 1. The material shows dendritic growth. As illustrated schematically in Fig. 1a, the primary dendrites are about 200 μm in width and grew along the ⟨001⟩ crystal direction. Grain boundaries, defined by boundaries with misorientation angles of 15° and above, were almost all parallel to the primary dendrite growth direction (indicated as the *Y*-direction). Transverse grain boundaries were essentially absent, and the resulting grain widths ranged from 200 μm to 2 mm. The superalloy was composed mainly of $Ni_3(Al, Ti)$ γ′-precipitates with ordered $L1_2$ structure within the solid-solution-strengthened γ-matrix with face-centered cubic structure. The volume fraction of the cuboidal γ′-particles was about 70%, and they precipitated coherently within the γ matrix obeying the cube-on-cube orientation relationship, $(001)_{\gamma'}//(001)_{\gamma}$ and $\langle 100\rangle_{\gamma'}//\langle 100\rangle_{\gamma}$ [26]. The cuboids were distributed regularly in the γ matrix, which appeared as interconnected 3D channels separating the cuboids. MC and $M_{23}C_6$ carbides were detected in the superalloy. Since their combined volume fraction is less than 1%, their impacts on the mechanical properties are not considered in this study.

Besides newly manufactured blades, LSP is also used for repair of blades after some time in service. To mimic the latter, the superalloy investigated in this study was prior to LSP vibration fatigued with a peak stress of about 257 MPa for 10^7 cycles to simulate service conditions, following the standard of the Ministry of Aviation Industry of the P.R.C. (HB5277-84), using the electric vibration test system produced by Suzhou Test Instrument Co., Ltd. The vibration fatigued specimen constituted a simulating blade and a holding end, with an arc chamfer between them. The sizes of the simulating blade and the holding end were $41 \times 20 \times 2$ mm^3 and $30 \times 24 \times 20$ mm^3, respectively. The γ′ precipitates maintained cuboidal shape after fatigue testing throughout the specimen (see Fig. 1d, which shows their morphology after etching off the γ-phase matrix), although their size and morphology varied from the dendrite cores to the interdendritic regions due to the well-known segregation of the γ′-forming elements as a result of solidification [27]. During fatigue, dislocations were generated with an average density of about 4×10^{14} m^{-2} (Fig. 1e). After vibration fatigue, LSP was carried out on the surface of a small part ($20 \times 20 \times 2$ mm^3) cut from the simulating blade about 1 cm above the root. The surface to be LSP treated was mirror polished using SiC papers of grits varying from #180 to #2400. A 0.125 mm thick aluminum foil was used as protective and absorbing layer, and water was applied as confining overlay to promote the generation of shock waves. The specimen was laser shock peened using a Q-

Table 1
Nominal composition of DZ417G Ni-based superalloy (wt. %).

Composition	Co	Cr	Al	Ti	Mo	V	Fe	C	B	Ni
Content	9.0–11.0	8.5–9.5	4.8–5.7	4.1–4.7	2.5–3.5	0.6–0.9	≤ 0.5	0.13–0.22	0.012–0.024	Balance

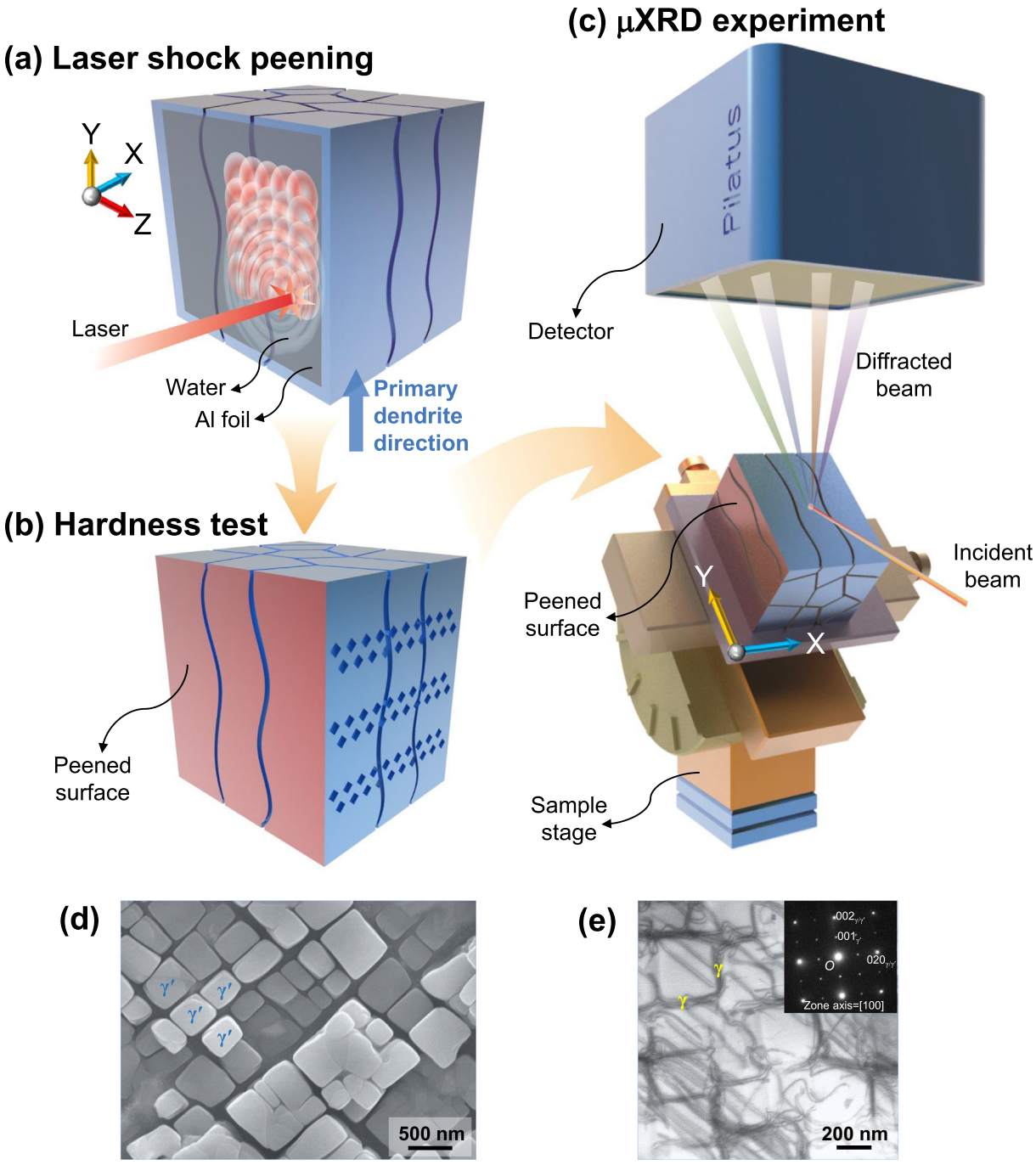

Fig. 1. Schematic diagrams showing the set-up for LSP, hardness testing and μXRD, with the aid of a Cartesian coordinate system *O-XYZ*. (a) LSP is carried out on the *YZ*-surface with the peening direction perpendicular to the primary dendrite growth direction. Grain boundaries, parallel to the primary dendrites, are indicated using the dark blue curves. After LSP, (b) hardness and (c) μXRD are conducted on a cross-sectional *XY*-plane. (d) and (e) reveal γ′ precipitates and dislocations in the microstructure of the superalloy after fatigue testing and prior to LSP.

switched Nd:YAG laser system. The shock peening direction (indicated as *X*-direction in Fig. 1a) was perpendicular to the dendritic growth direction. LSP was performed with the processing parameters listed in Table 2, an overlapping rate of 50% and repeated three times.

2.2. Hardness measurement

Three regions were arbitrarily chosen on the cross sectional *XY*-plane of the specimen after LSP to investigate the depth dependence of the hardness (illustrated in Fig. 1b). In each region, the

Table 2
Processing parameters used for LSP.

Laser energy	Spot diameter	Pulse width	Frequency	Power density
5.6 J	2.2 mm	20 ns	1 Hz	7.4 GW/cm^2

Vickers hardness was measured along two lines approximately 100 μm separated from each other, both parallel to the peening direction using a HXD-1000TMC/LCD instrument, with a load of 200 gf and a dwell time of 30 s. A total of 14–15 indentations were performed along each line. The distance between two adjacent indents was fixed at 120 μm (Fig. 1b). On one line, the first indent was placed at a depth of 60 μm from the surface, while at 120 μm from the surface on the other. The diagonal length of the indents was about 30 μm, i.e., less than one-fourth of the space between adjacent indents, which is considered sufficient to eliminate overlap of the deformation zones between neighbouring indents [28]. To establish the benchmark for comparison, the hardness distribution was also measured along a line from surface to interior on the vibration-fatigued Ni-based superalloy without LSP.

2.3. Synchrotron μXRD

Synchrotron polychromatic μXRD (also known as Laue μXRD) was carried out at beamline 12.3.2 of the Advanced Light Source at Lawrence Berkeley National Laboratory [29]. In this setup, a pair of Kirkpatrick-Baez mirrors was used to focus polychromatic X-ray beam (5–24 keV) to a size of about 1 × 1 μm^2. The samples were glued on a high-accuracy *XY* scan stage that was inclined 45° with respect to the incident X-ray beam. An area of 1705 × 234 μm^2 on the *XY*-plane was scanned with the polychromatic X-ray beam with a step size of 5 μm along the peening direction (*X*-direction) and 3 μm along the dendrite growth direction (*Y*-direction). At each scan position, a Laue pattern was recorded using a two-dimensional Pilatus-1 M detector (DECTRIS, Baden-Dättwil, Switzerland), mounted in 90° reflection geometry about 150 mm above the sample (Fig. 1c). All 26,598 recorded Laue patterns were analysed using the software package XMAS [30], adopting the custom-developed peak position comparison method [31].

To analyse the peak shape in Laue μXRD, the 004 diffraction peak was converted from detector coordinates to reciprocal space coordinates 2θ-χ (Fig. 2a and b), where 2θ is the diffraction angle between incident and diffracted beam, while χ is the angle between the diffraction plane defined by the incident and the diffracted beam and the plane defined by the incident beam and the detector normal. The intensity distributions in the 2θ-χ space usually appear anisotropic with an elliptical shape. Therefore, for the intensity distribution of each peak in reciprocal space coordinates 2θ-χ, the long and short axes were determined. The full widths at half maximum (FWHMs) of the intensity profiles along these long and short axes are denoted as β_L and β_S, respectively (Fig. 2c and d). In the present Laue diffraction experiment, the 00 *N* reflection signals (*N* = 2, 4, 6, 8) from the γ phase and the 00 *M* reflections (*M* = 2, 3, 8, 9) from the γ′ phase appeared at the same position. Therefore, reference to a certain peak such as 004 (to comply with following monochromatic investigations), actually means the superposition of several contributing harmonic reflections.

In order to determine locally the radial line profile of the diffraction peaks for quantification of the dislocation density [32,33], mapping was performed using a monochromatic beam by scanning the X-ray energy in minute energy steps, which is termed energy scans in this article. For the present study, the 004 peak was chosen for energy scan in the range of 9950–10250 eV with a step size of 1 eV on Beamline 21A at the Taiwan Photon Source. The measurements were conducted in a depth range of 0 to 1.7 mm along two lines that were 100 μm apart from each other and parallel to the peening direction on the *XY*-plane. Based on the energy scan, the dependence of the raw radial intensity profile (black circles in Fig. 3) on the diffraction vector $Q = 4\pi\frac{\sin\theta}{\lambda}$, where λ is the wavelength and θ the Bragg angle, was determined. After fitting the experimental data, the radial line profile was decomposed into two sub-profiles, representing the diffraction signals from γ and γ′ phases (orange and green curves, respectively, in Fig. 3). For decomposition, it was assumed that the integrated intensity ratio of the two sub-profiles was equal to the ratio between the volume fractions of the corresponding phases, i.e., 30:70 between γ and γ′ phase. The FWHMs for both the phases, δ_γ and $\delta_{\gamma'}$, were then determined for quantification of the dislocation density using the procedure outline in [34], which was adapted from the classical Wilkens' theory [35]. Further details about peak fitting and dislocation density calculations can be found in Ref. [34].

2.4. Electron microscopy

To observe the morphology of the γ′ precipitates and their spatial distribution in the γ matrix, *XY*-plane section of the specimens

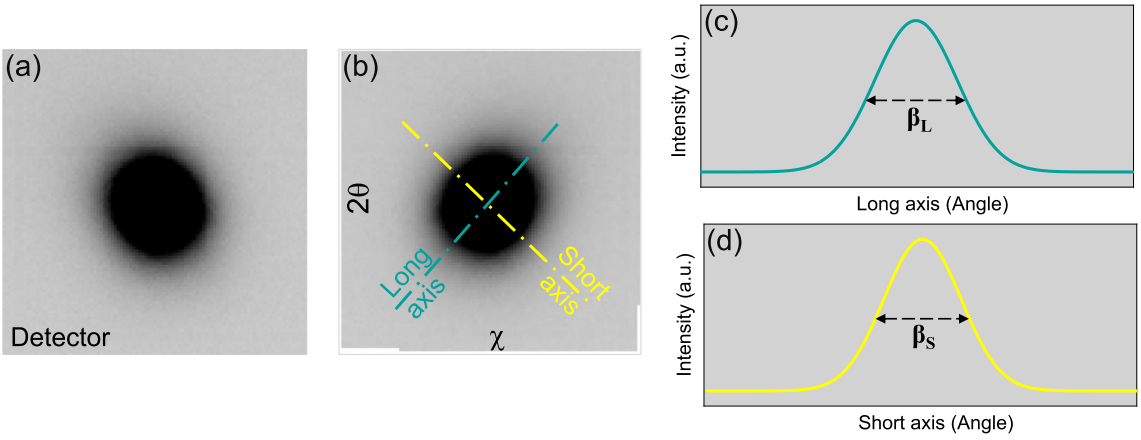

Fig. 2. An example illustrating how the shape of the Laue diffraction peak is quantified. A 004 Laue diffraction peak is (a) presented in detector coordinates and (b) converted into 2θ-χ coordinates. The corresponding intensity profiles along the long and the short axes are displayed in (c) and (d), respectively.

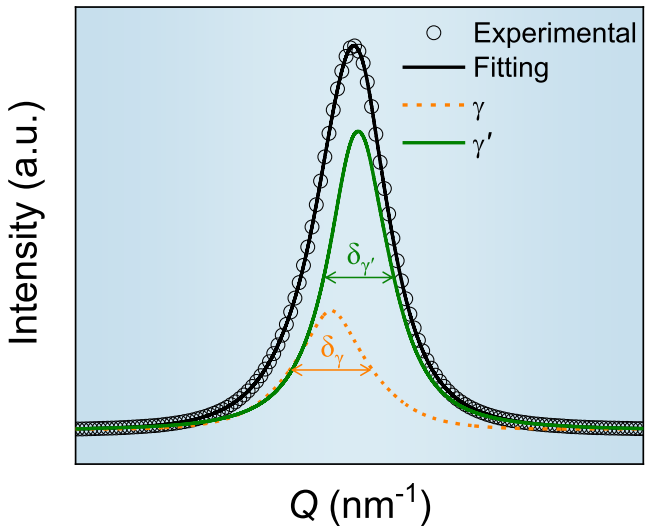

Fig. 3. Radial line profile of a 004 peak of the Ni-based superalloy determined from an energy scan with monochromatic X-ray beam. The black circles represent experimental diffraction data at a particular position, while the black curve is a fit to the circles using multiple Gaussian function. The orange and green sub-profiles originating from γ and γ′ phases, respectively, are obtained by decomposition of the black profile following the procedure described in [34].

was electrochemically etched in H_3PO_4 aqueous solution (25%:75%) under a constant voltage of 5 V to etch off the γ phase. A Hitachi SU6600 field emission scanning electron microscope (SEM) was used for imaging the cuboidal γ′ precipitates at various depths along the peening direction on the cross section. Their individual sizes were determined as geometric mean of the lengths of two of each cuboid's adjacent sides. To observe dislocations in the fatigued superalloy, a TEM foil was prepared by twin-jet electropolishing in $HClO_4$ alcohol solution (10%:90%) and then characterized using a JEM-2100F field emission TEM with a 200 kV accelerating voltage.

3. Results

3.1. Hardness profile

The microhardness profile from surface to interior along the peening direction is shown in Fig. 4. The hardness of the fatigued Ni-based superalloy without LSP is measured to be (396 ± 11) HV0.2, as indicated by the solid cyan dots in Fig. 4. It is unequivocally demonstrated that no long-range hardness gradient, but only a small variation in hardness values is revealed in the fatigued superalloy. In contrast, LSP induces a significant increase in hardness, which is about 50% higher near the peened surface (587 HV0.2); the case, defined as the region in which an increased hardness is detected, ranges from the surface to a depth of about 1.2 mm.

3.2. Laue μXRD

The patterns obtained by the Laue μXRD are evaluated in two ways. The peak positions allow determination of the local crystallographic orientations, and the shape of the peaks acts as an initial manifestation of the presence of dislocation structure. The crystallographic orientations in the area scanned by polychromatic X-rays are displayed in Fig. 5a, where the colours represent the crystallographic directions along the *Z*-direction, i.e., normal of the cross section. Two large grains are identified in the examined area by their appearance in different colours in the map (Grain 1 in red and Grain 2 in orange). The alternating appearance of both colours in the region on the right is due to the co-existence of both grains in the volume penetrated by the synchrotron X-ray beam and giving rise to diffraction. Only the orientation from the grain dominating the diffraction signal, i.e., with larger volume fraction along the path of the incoming X-rays, is presented in Fig. 5a. The exact location of the grain boundary between these two grains in 3D is unknown, which however is less important for the present analysis. No other orientation is detected in the mapped region. Apparently, the original grain structures are preserved and no grain refinement occurred.

Three typical Laue diffraction patterns taken at various depths from the peened surface at positions marked by B, C and D in Fig. 5a are shown in Fig. 5b, c, and d, respectively. The diffraction peaks obtained from the location close to the peened surface (position B) are significantly broadened compared to those obtained from the same grain but about 1 mm away from the surface (position C), because a large number of dislocations are generated by LSP near the surface. The diffraction peaks from the second grain (position D) are comparatively sharp and intense. The misorientation profiles along the lines marked E1-E2 and F1-F2 on Fig. 5a are displayed in Fig. 5e. The majority of the misorientation angles between neighbouring pixels is below 1.5°. The point-to-origin misorientation angle increases to about 2° from the peened surface to a depth of about 150 μm, indicating an accumulation of misorientation over this distance. In larger distances from the surface, i.e., in deeper regions of Grain 1, the point-to-origin misorientation angle remains this high level. The observed scatter is caused by occurring point-to-point misorientations.

The 004 reflection is selected for further peak shape analysis for two reasons. Firstly, it is the strongest peak and has a high signal-to-noise ratio. Secondly, it is observed in both of the detected orientations (marked by the red circles in Fig. 5b, c and d). The peak widths along the short (β_S) and long (β_L) axes determined at each position in the scanned area are plotted in Fig. 6a and b, respectively. Both widths decrease with increasing distance from the peened surface, revealing a depth dependence of the local dislocation densities in the LSP treated superalloy. The ratio of β_S to β_L at each position in the scan is computed and displayed in Fig. 6c. Up to a depth of about 1.1 mm, i.e., in Grain 1, it is close to 1, implying a near-isotropic diffraction peak broadening. The ratio in Grain 2 is generally lower (about 0.5), reflecting that the intensity distributions of the 004 diffraction peaks in the 2θ-χ coordinates are slightly elliptical. The β_S/β_L ratio varies significantly within each grain. Moreover, the peak widths and β_S/β_L ratios are affected by the presence of interdendritic carbides, as pointed out by the black arrows, due to different levels of plastic deformation close to the carbides [36].

3.3. Energy scans with monochromatic beam for dislocation characterization

From the energy scans with monochromatic X-rays, the radial line profile of diffraction peak 004 is obtained and separated into sub-profiles for each phase, based on which values of FWHM and dislocation density are determined. The FWHMs of these radial sub-profiles, δ, as a function of distance from the peening surface are shown in Fig. 7a. At positions deeper than 200–300 μm below the peened surface, the FWHM obtained for the γ phase is larger than that for the γ′ phase. Near the peened surface, FWHMs for both phases are similar.

Following the recently developed procedure [34], the redundant dislocation densities ρ were determined locally in each of the two phases based on the radial sub-profile in dependence of the depth below the peened surface (Fig. 7b). In the spirit of Weertman [37], the dislocation density is split into the redundant dislocation den-

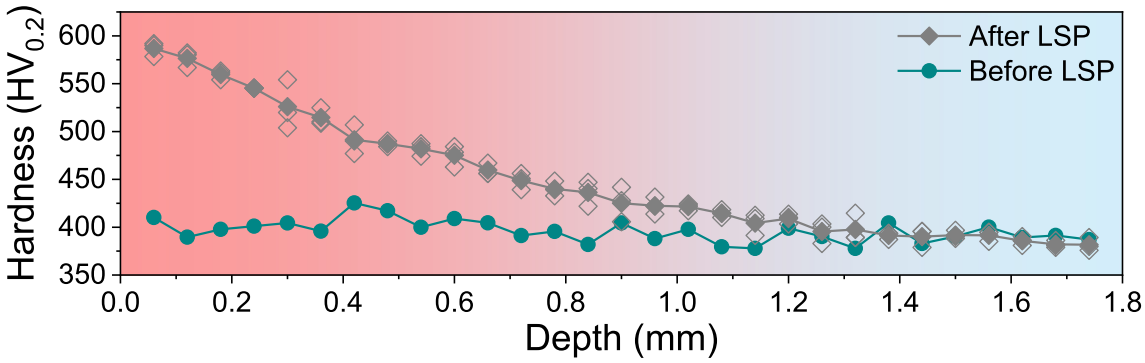

Fig. 4. Variation of the Vickers microhardness as a function of the peening depth of the laser shock peened Ni-based superalloy. The hollow diamonds are the data measured while the solid diamonds are their average values. The solid cyan dots represent the hardness of the fatigued superalloy without LSP.

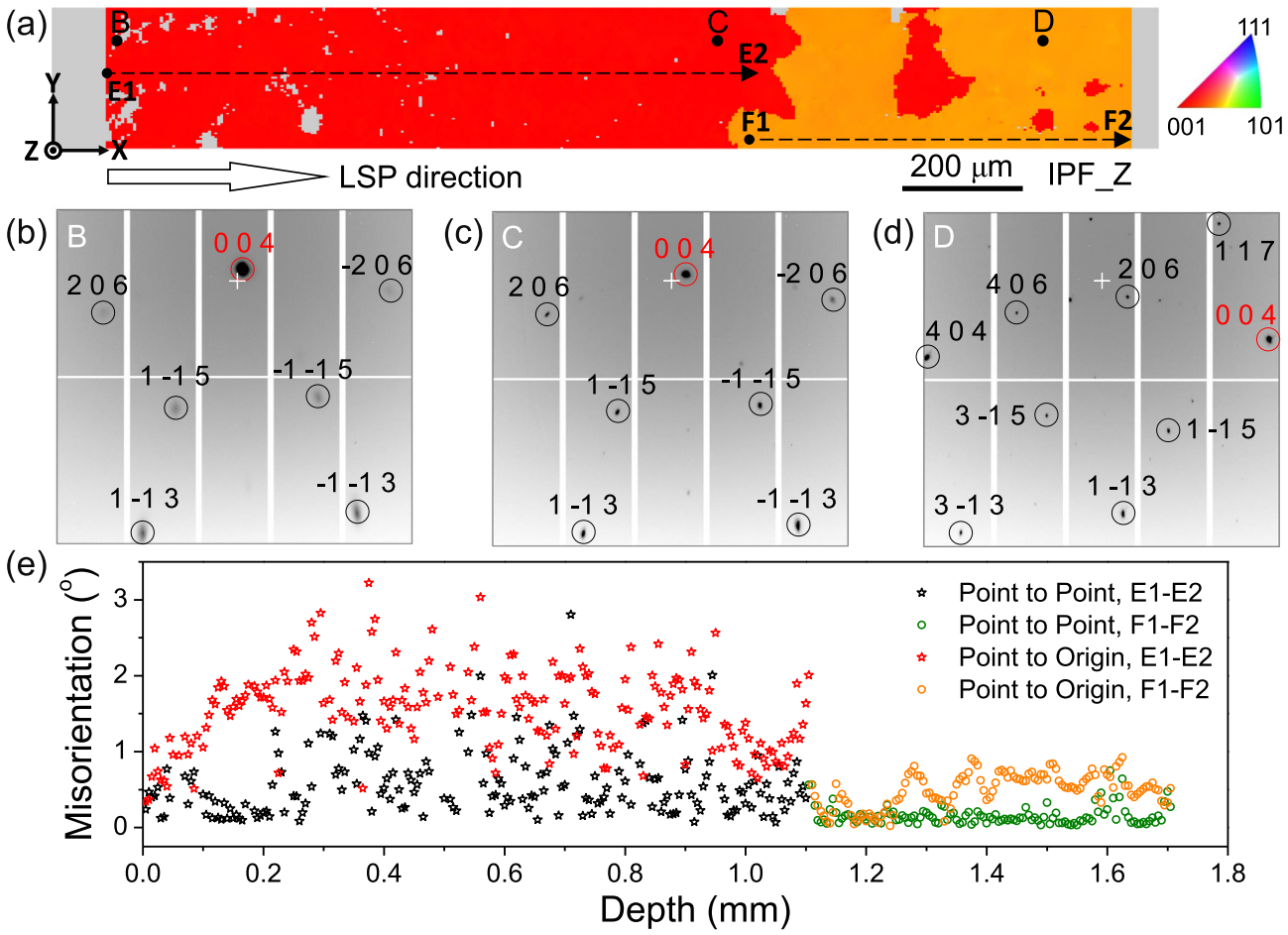

Fig. 5. Laue μXRD on the cross section of the laser shock peened Ni-based superalloy. (a) Orientation map, colored according to the crystallographic orientation along the *Z*-direction. The peened sample surface is to the left, non-indexed pixels are shown in grey. (b)-(d) Three representative indexed Laue diffraction patterns collected at positions B, C and D marked in (a), respectively. The white cross in each Laue pattern marks the position where the beam is diffracted by a diffraction angle 2θ of 90° and χ of 0°. (e) Misorientation profiles along the peening direction in the two grains, marked E1-E2 and F1-F2. Both point-to-origin (with respect to E1/F1) and point-to-point misorientations are shown.

sity which has no geometrical consequences on a microscale and the non-redundant dislocation density giving rise to lattice curvature or gradients in the elastic strain. Similar to the depth-dependent variations in FWHM for both the phases, higher dislocation densities are detected in γ phase than in γ′ phase in most regions except close to the surface. In the regions unaffected from LSP (deeper than 1.2 mm from the peened surface), the average dislocation density in the γ phase is 14.6×10^{14} m^{-2}, while it is only 5.3×10^{14} m^{-2} in the γ′ phase. These dislocations are introduced during the vibration fatigue test [34]. The dislocation density in the γ′ phase increases continuously from the unaffected interior to a depth of 100 μm. Within the region up to 100 μm from the peened surface, the dislocation density is constant, or even drops slightly. For the γ phase, the dislocation densities increase from low values at 1.2 mm from the surface and deeper to an almost constant value in a depth range between 100 and

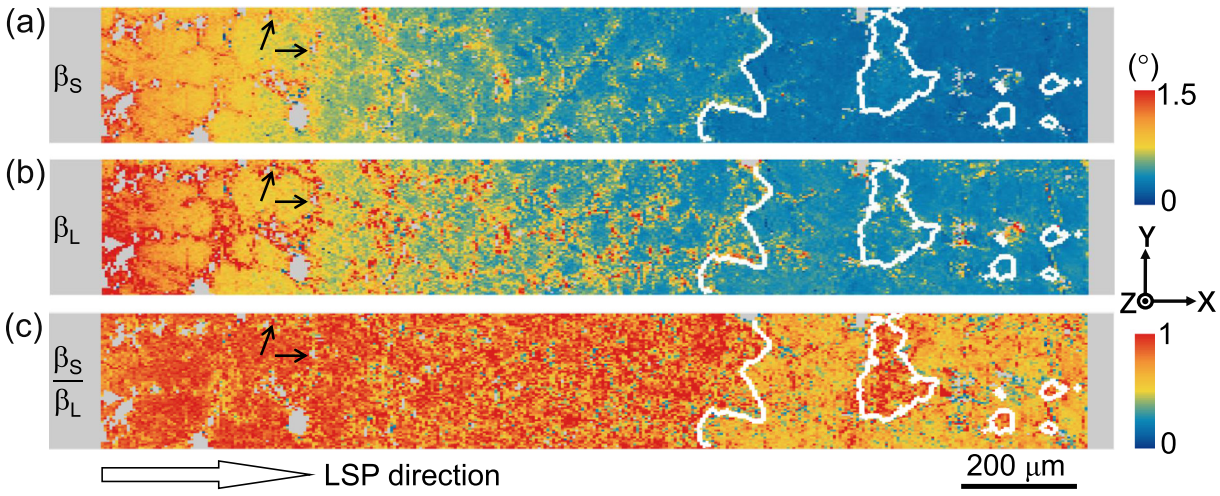

Fig. 6. Quantitative results of the 004 Laue diffraction peak in the laser shock peened Ni-based superalloy. Maps of peak widths (a) along short and (b) long axes and (c) their ratios of the 004 Laue peak in the laser shock peened Ni-based superalloy. The white curves correspond to colour changes between red and orange in the orientation map, i.e., the high angle grain boundaries.

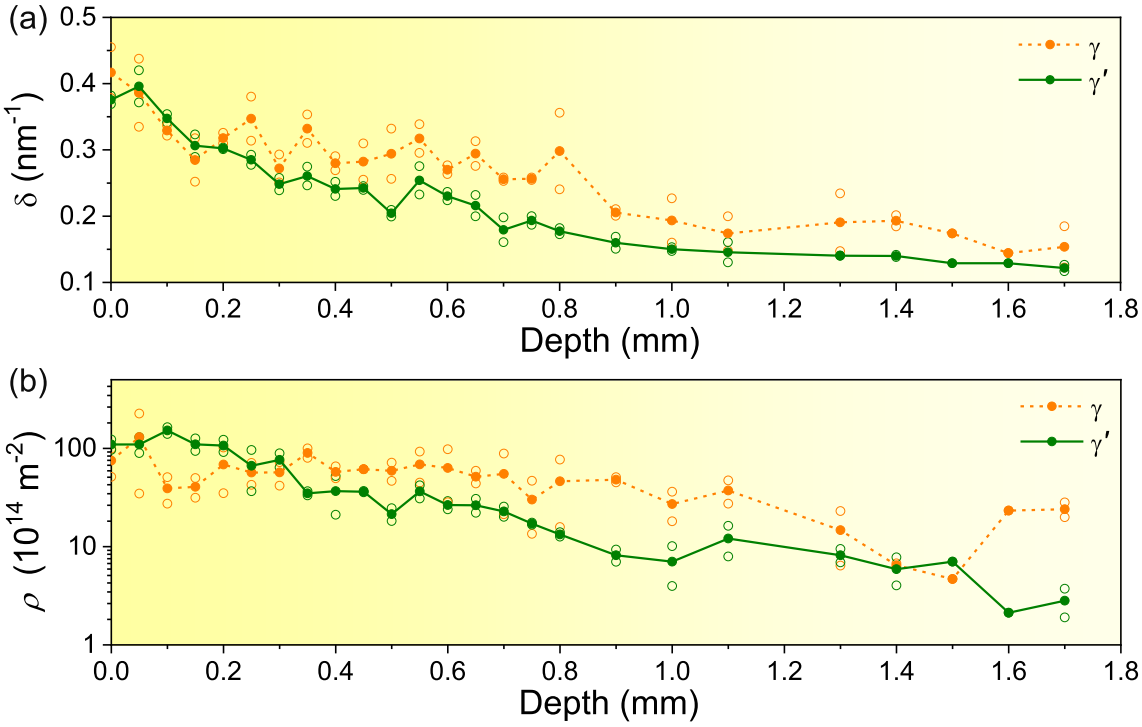

Fig. 7. Quantitative results based on monochromatic energy scans. (a) FWHM δ and (b) redundant dislocation density ρ obtained from energy scans for both γ and γ′ phases as a function of depth in the peened case. Hollow circles represent the original data from two individual measuring lines, while solid dots indicate average values.

800 μm. The two trends of the dislocation densities cross each other at the depth around 300 μm (Fig. 7b), leading to a lower dislocation density in the γ phase than in the γ′ phase in a region between 100 and 300 μm below the peened surface. In the region up to 200 μm below the peened surface, the average dislocation densities detected in γ and γ′ phases are 7.1×10^{15} and 11.8×10^{15} m^{-2}, respectively. These are about 5 and 20 times higher than the respective values in the unaffected region.

3.4. Microscopic observations

The shape and size of γ′ precipitates after LSP were investigated in a cross section using SEM. The overall shape of γ′ precipitates remained cuboidal, despite occasional coalescence (Fig. 8a and b). As seen from Fig. 8c, the sizes of the γ′ cuboids range around an average of 360 nm and do not show any noticeable systematic variation within the investigated region, i.e., the case formed by LSP.

4. Discussion

As the present study illustrates, synchrotron μXRD is a powerful tool for quantitative analysis of the local microstructures. The small beam size of 1×1 μm^2 micrometer ensures a high spatial resolution. Based on the Laue diffraction patterns collected with a polychromatic beam, both the crystallographic orientation and

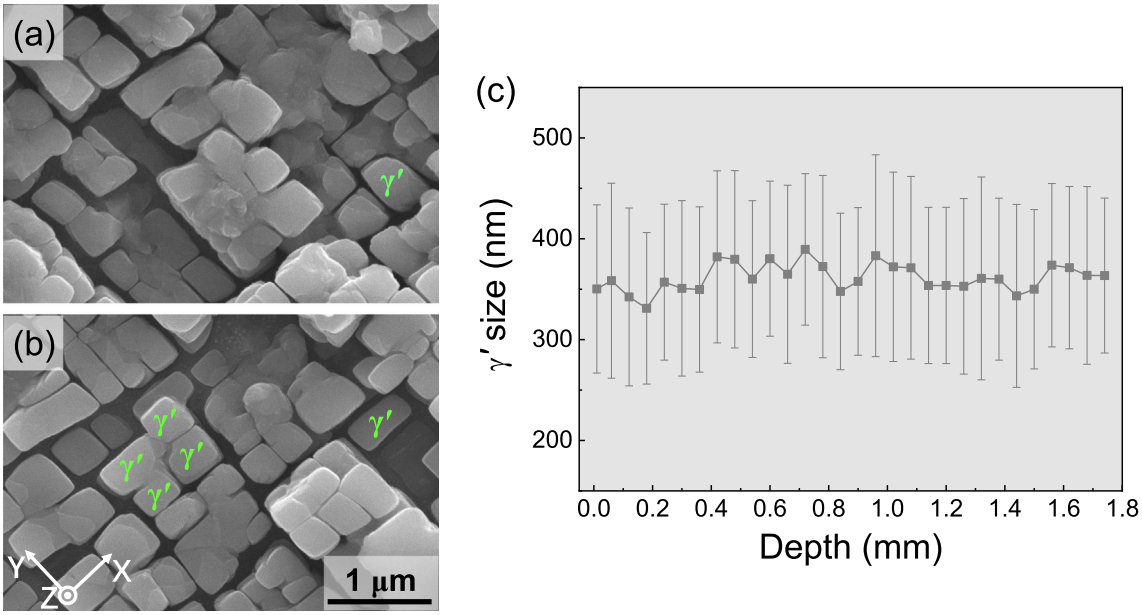

Fig. 8. SEM investigation of the γ′ precipitates. The secondary electron images are taken at a depth of (a) about 10 μm and (b) 1.0 mm. (c) shows the size of the γ′ cuboids in dependence on depth. At each depth, 96 cuboidal γ′ particles are measured. The error bars represent the standard deviation of their size distributions.

the shape of the peaks can be determined. When using the monochromatic beams, dislocation density, lattice parameter, and residual elastic strain of different microstructural phases can be quantified separately, even for cases like the present Ni-based superalloy where the two phases have similar lattice parameters. It is evident that μXRD can be used for studying severely deformed samples containing dislocation densities in the order above 10^{15} m^{-2}, which is challenging to quantify by TEM.

With a suitable sub-profile separation and analysis algorithm, the local dislocation densities in both γ and γ′ phases in the present DZ417G superalloy within the laser shock peened case are quantified. Such information is crucial for understanding the plastic deformation induced by LSP and for quantifying the contribution of each phase to the strength enhancement caused by LSP.

4.1. LSP induced plastic deformation

The hardness and synchrotron μXRD data reveal that in the region up to 1.2 mm from the peened surface a case is formed by LSP where both the hardness and the dislocation density, are higher than those in the interior. The size and morphology of γ′ precipitates are the same throughout the case, proving that no pronounced phase transformation between γ and γ′ phases occurs during LSP. Also, no grain refinement is observed, which is similar to what has been reported in LSP treated mono- and polycrystalline Ni-based superalloys [9,38,39] as well as other materials systems [40,41]. The LSP induced hardening is therefore mainly caused by dislocations.

The nearly isotropic broadening of the Laue peaks in the 2θ-χ space (see Fig. 6) suggests that the dislocations generated by LSP are mainly redundant, and a small fraction of non-redundant [42]. The non-redundant dislocation content to produce a misorientation ϕ across a distance d as in the orientation gradient near the surface is given by the Read Shockley equation $\rho = \phi / bd$ and determined by the Burgers vector b of the dislocations [43]. Fig. 5e shows an orientation gradient accumulating a misorientation angle of 2° across a distance of 150 μm below the peened surface, resulting in a non-redundant dislocation density of 9.2×10^{11} m^{-2}. At a larger depth, the misorientation angle of 2° with respect to the orientation at the surface does not vary systematically. Similar orientation gradients within a similar range of depth have also been observed in LSP treated Ti6Al4V [44] and Inconel 718SPF [45]. Even the non-redundant dislocation density 2.1×10^{13} m^{-2} expected locally from the point-to-point misorientation angle of 1.5° between points at a distance of 5 μm is 2 orders of magnitude lower than the redundant dislocation density (Fig. 7b). Consequently, the non-redundant dislocation density is negligible and hence redundant dislocations dominate the total dislocation density. The latter affect the mechanical properties to a much larger depth than the non-redundant dislocations, which are responsible for the orientation gradient close to the surface.

The dislocations are distributed heterogeneously between the γ and γ′ phases. For depths deeper than 0.7 mm from the surface, the dislocation density in the γ channels is approximately twice that in the γ′ cuboids. In the region close to the peened surface, the dislocation density in the γ channels remains constant, probably due to dynamic annihilation, while the dislocation density is higher in the γ′ cuboids. The annihilation of dislocations in the γ channels becomes easier as the dislocations are confined, while the $L1_2$ structure of the γ′ cuboids makes annihilation difficult as the motion of superdislocations is restricted to their slip plane by an anti-phase boundary.

The dislocation density revealed in DZ417G is much higher than the ones reported for Ni and other Ni-based superalloys after shock loading. For example, after shock loading with a pressure of 25 GPa, a dislocation density of 1.3×10^{15} m^{-2} in single phase Inconel 600 is reported [46]. This dislocation density is only about 1/5 of that in the γ channels of the present sample. Both the presence of dislocations prior to LSP and the pinning by γ′ cuboids may be important factors for this difference.

4.2. Strengthening mechanism

In general, the strength of a metallic alloy is a combined effect of solute atoms, dislocations, grain boundaries, and precipitates [47]. Since no new grain boundaries are generated by LSP in our study and the precipitate size and morphology throughout the case are the same as those in the interior, the effects of grain boundaries

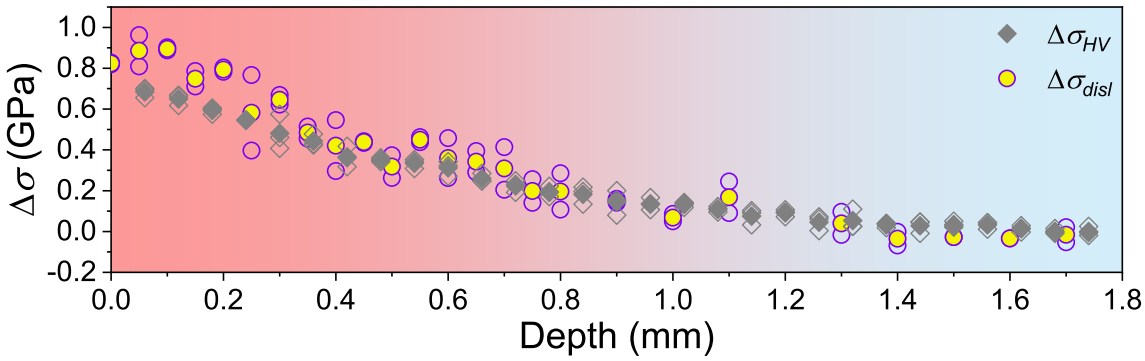

Fig. 9. Strength contribution of redundant dislocations induced by LSP in comparison with hardness increase depending on the depth from the peened surface. Hollow symbols display values obtained locally at different lines, while solid ones represent their average values.

and precipitates are ruled out for explaining the observed hardness increase. Likewise, hardness differences in the case caused by different solid solution strengthening can be excluded as no hint of any partial or full dissolution of the γ′ precipitates is demonstrated and long range migration and redistribution of solute elements are not likely to occur in the short period of time of LSP. Consequently, the observed hardness profile must solely be due to the variations in the local dislocation densities caused by LSP.

The contribution of the dislocation-dislocation interactions to the flow stress is described by the Taylor's relation [48]:

$$\Delta\sigma_{disl} = \alpha M G b\sqrt{\rho} \tag{4}$$

where α is an interaction coefficient, M the Taylor factor, G the shear modulus, b the Burgers vector, and ρ the total dislocation density. The contributions from the γ and γ′ phases are considered separately obeying the rule of mixtures:

$$\Delta\sigma_{disl} = f_{\gamma}\Delta\sigma_{disl,\gamma} + (1 - f_{\gamma})\Delta\sigma_{disl,\gamma'} \tag{5}$$

where f_{γ} is the volume fraction of the γ phase (30%). Using the redundant dislocation densities determined (and presented in Fig. 7b) and the values α = 0.24, M = 2.449, b = 0.253 nm, G = 76 GPa for the γ phase and 78 GPa for the γ′ phase in Equation (5) [49], the strength increase (compared to the unaffected interior) contributed by the dislocations in the peened case are estimated. They are compared with the hardness increase ΔHV with respect to the average value for an unpeened, fatigued specimen reported in Fig. 4 converted to a contribution to the tensile strength $\Delta\sigma_{HV}$ by Tabor's relation: $\sigma_{HV} = HV/3$ [50].

As seen from Fig. 9, the calculated strengthening effect $\Delta\sigma_{disl}$ from the determined dislocation densities agrees well with the observed strength increase $\Delta\sigma_{HV}$ determined from the hardness, proving that work-hardening by dislocations is responsible for the hardness increase in the case of the laser shock peened Ni-based superalloy DZ417G in this study. A deviation is seen for the first 300 μm below the peened surface, which is probably due to the heterogenous dislocation density in the phases and may indicate that there is an overestimation of the resolved dislocation densities due to the difficulties with profile separation in this case.

5. Conclusions

In the present study, a laser shock peened Ni-based superalloy DZ417G was characterized using advanced synchrotron μXRD with the aim to analyse and quantify the relevant strengthening mechanism. The main conclusions are:

(1) LSP develops a hardened case in the Ni-based superalloy to a depth of 1.2 mm from the peened surface. After three impacts, a maximum hardness of 587 HV0.2 is obtained close to the surface, which is about 50% higher than that in the unaffected region.
(2) Plastic deformation caused by LSP results in a high redundant dislocation density. Only a small density (2.1×10^{13} m^{-2}) of non-redundant dislocations are required as determined from the local misorientations.
(3) The redundant dislocation densities induced by LSP near the surface regions reach 7.1–11.8 $\times$ 10^{15} m^{-2} in γ and γ′ phases, which is about 5 and 20 times higher than that in the unaffected region. The redundant dislocation density in the γ phase remains a plateau value between 100 μm and 800 μm depth from the surface, while the dislocation density in the γ′ cuboids increase continuously from the unaffected region towards the surface except the first 100 μm from the surface.
(4) The work-hardening effect of the redundant dislocation density induced by LSP is quantified based on the μXRD measured dislocation densities. The excellent agreement with the local hardness measurements confirms accumulation of dislocations as the dominant strengthening mechanism.

Declaration of Competing Interest

The authors declare that they have no known competing financial interests or personal relationships that could have appeared to influence the work reported in this paper.

Acknowledgements

This work was supported by the National Science and Technology Major Project (2019-VII-0019-0161), National Natural Science Foundation of China (No. 51927801 and U2032205), and 111 Project 2.0 (BP0618008). G.Z. would like to acknowledge the financial support from the program of China Scholarships Council (No. 201806280355). K.C. appreciates the support from the International Joint Laboratory for Micro/Nano Manufacturing and Measurement Technologies and the Collaborative Innovation Center of High-End Manufacturing Equipment. Y.Z. acknowledges support from the European Research Council (ERC grant agreement No. 788567 M4D).

Author contributions

Chen K provided the research funding, the supervision, the depth analysis and the revision. Zhou G designed the study, performed the experiments, analyzed the data and wrote the manuscript. Zhang YB and Pantleon W offered the theoretical analysis and revised the manuscript. Kou JW helped with the data analysis. Luo SH and He WF supported the materials. Ku CS, Chiang CY and Tamura N assisted in the synchrotron microdiffraction experiment. Ramamurty U and Tan XP smoothed the manuscript.

References

[1] R. Schafrik, R. Sprague, Gas turbine materials, Adv. Mater. Process 5 (2004) 29–34.
[2] T.M. Pollock, Alloy design for aircraft engines, Nat. Mater. 15 (2016) 809–815.
[3] T.M. Pollock, S. Tin, Nickel-based superalloys for advanced turbine engines: chemistry, microstructure and properties, J. Propuls. Power 22 (2006) 361–374.
[4] M. Ciavarella, G. Demelio, A review of analytical aspects of fretting fatigue, with extension to damage parameters, and application to dovetail joints, Int. J. Solids Struct. 38 (2001) 1791–1811.
[5] D. Thomson, The national high cycle fatigue (HCF) program. Third National Turbine Engine High Cycle Fatigue Conference, 1998.
[6] S. Bagheri, M. Guagliano, Review of shot peening processes to obtain nanocrystalline surfaces in metal alloys, Surf. Eng. 25 (2009) 3–14.
[7] A.H. Clauer, Laser shock peening for fatigue resistance, Surf. Perform. Titan 217 (1996) 230.
[8] C.S. Montross, T. Wei, L. Ye, et al., Laser shock processing and its effects on microstructure and properties of metal alloys: A review, Int. J. Fatigue 24 (2002) 1021–1036.
[9] A. Gill, A. Telang, S.R. Mannava, et al., Comparison of mechanisms of advanced mechanical surface treatments in nickel-based superalloy, Mater. Sci. Eng., A 576 (2013) 346–355.
[10] P. Peyre, R. Fabbro, P. Merrien, et al., Laser shock processing of aluminium alloys. Application to high cycle fatigue behaviour, Mater. Sci. Eng., A 210 (1996) 102–113.
[11] U. Sánchez-Santana, C. Rubio-González, G. Gomez-Rosas, et al., Wear and friction of 6061–T6 aluminum alloy treated by laser shock processing, Wear 260 (2006) 847–854.
[12] S.A. Kumar, R. Sundar, S.G.S. Raman, et al., Fretting wear behavior of laser peened Ti-6Al-4V, Tribol. Trans. 55 (2012) 615–623.
[13] A.S. Gill, Z. Zhou, U. Lienert, et al., High spatial resolution, high energy synchrotron x-ray diffraction characterization of residual strains and stresses in laser shock peened Inconel 718SPF alloy, J. Appl. Phys. 111 (2012) 084904.
[14] S. Amini, M. Dadkhah, R. Teimouri, Study on laser shock penning of Incoloy 800 super alloy, Optik 140 (2017) 308–316.
[15] W.F. He, Y.H. Li, Q.P. Li, et al., The effects of laser shock peening on fatigue life in Ni-based superalloy, Adv. Mater. Res. 135 (2010) 209–214.
[16] Y. Fang, Y. Li, W. He, et al., Numerical simulation of residual stresses fields of DD6 blade during laser shock processing, Mater. Des. 43 (2013) 170–176.
[17] Y. Li, L. Zhou, W. He, et al., The strengthening mechanism of a nickel-based alloy after laser shock processing at high temperatures, Sci. Technol. Adv. Mater. 14 (2013) 055010.
[18] A.S. Gill, A. Telang, V.K. Vasudevan, Characteristics of surface layers formed on inconel 718 by laser shock peening with and without a protective coating, J. Mater. Process. Technol. 225 (2015) 463–472.
[19] J.Z. Lu, K.Y. Luo, Y.K. Zhang, et al., Grain refinement mechanism of multiple laser shock processing impacts on ANSI 304 stainless steel, Acta Mater. 58 (2010) 5354–5362.
[20] J.Z. Lu, K.Y. Luo, Y.K. Zhang, et al., Grain refinement of LY2 aluminum alloy induced by ultra-high plastic strain during multiple laser shock processing impacts, Acta Mater. 58 (2010) 3984–3994.
[21] L. Chen, X. Ren, W. Zhou, et al., Evolution of microstructure and grain refinement mechanism of pure nickel induced by laser shock peening, Mater. Sci. Eng., A 728 (2018) 20–29.
[22] L. Chen, Y. Sun, L. Li, et al., Microstructural evolution and mechanical properties of selective laser melted a nickel-based superalloy after post treatment, Mater. Sci. Eng., A 792 (2020) 139649.
[23] M. Rozmus-Górnikowska, J. Kusiński, Ł. Cieniek, et al., The microstructure and properties of laser shock peened CMSX4 superalloy, Metall. Mater. Trans. A 52 (2021) 2845–2858.
[24] X. Chen, C. Dejoie, T. Jiang, et al., Quantitative microstructural imaging by scanning Laue x-ray micro- and nanodiffraction, MRS Bull. 41 (2016) 445–453.
[25] B.C. Larson, L.E. Levine, Submicrometre-resolution polychromatic three-dimensional X-ray microscopy, J. Appl. Crystallogr. 46 (2013) 153–164.
[26] R.C. Reed, C.M.F. Rae, Physical metallurgy of the nickel-based superalloys, in: D.E. Laughlin, K. Hono (Eds.), Physical Metallurgy, Elsevier, Oxford, 2014, pp. 2215–2290.
[27] U. Hemmersmeier, M. Feller-Kniepmeier, Element distribution in the macro- and microstructure of nickel base superalloy CMSX-4, Mater. Sci. Eng., A 248 (1–2) (1998) 87–97.
[28] ASTM International. Standard test method for Vickers hardness of metallic materials, 1992.
[29] M. Kunz, N. Tamura, K. Chen, et al., A dedicated superbend x-ray microdiffraction beamline for materials, geo-, and environmental sciences at the advanced light source, Rev. Sci. Instrum. 80 (2009) 035108.
[30] N. Tamura, XMAS: a versatile tool for analyzing synchrotron x-ray microdiffraction data, in: R.I. Barabash, G. Ice (Eds.), Strain and Dislocation Gradients from Diffraction: Spatially-Resolved Local Structure and Defects, Imperial College Press, London, 2014, pp. 125–155.
[31] J. Kou, K. Chen, N. Tamura, A peak position comparison method for high-speed quantitative Laue microdiffraction data processing, Scr. Mater. 143 (2018) 49–53.
[32] T.W. Cornelius, D. Carbone, V.L.R. Jacques, et al., Three-dimensional diffraction mapping by tuning the X-ray energy, J. Synchrotron Radiat. 18 (2011) 413–417.
[33] G. Zhou, J. Kou, Y. Li, et al., Quantitative Scanning Laue Diffraction Microscopy: Application to the study of 3D printed nickel-based superalloys, Quantum Beam Sci. 2 (2018) 13.
[34] G. Zhou, W. Pantleon, R. Xu, et al., Quantification of local dislocation density using 3D synchrotron monochromatic X-ray microdiffraction, Mater. Res. Lett. 9 (2021) 183–189.
[35] M. Wilkens, The determination of density and distribution of dislocations in deformed single crystals from broadened X-ray diffraction profiles, Phys. Status Solidi 2 (1970) 359–370.
[36] G. Liu, J.S. Cantó, S. Winwood, et al., The effects of microstructure and microtexture generated during solidification on deformation micromechanism in IN713C nickel-based superalloy, Acta Mater. 148 (2018) 391–406.
[37] J. Weertman, Dislocation based fracture mechanics, World Scientific, Singapore, 1996.
[38] D. Karthik, S. Swaroop, Laser shock peening enhanced corrosion properties in a nickel based Inconel 600 superalloy, J. Alloy. Compd. 694 (2017) 1309–1319.
[39] G.X. Lu, J.D. Liu, H.C. Qiao, et al., Effect of laser shock on tensile deformation behavior of a single crystal nickel-base superalloy, Mater. Sci. Eng., A 686 (2017) 46–53.
[40] I. Altenberger, E.A. Stach, G. Liu, et al., An in situ transmission electron microscope study of the thermal stability of near-surface microstructures induced by deep rolling and laser-shock peening, Scr. Mater. 48 (2003) 1593–1598.
[41] M.S. Schneider, B. Kad, D.H. Kalantar, et al., Laser shock compression of copper and copper-aluminum alloys, Int. J. Impact Eng. 32 (2006) 473–507.
[42] G.E. Ice, R.I. Barabash, White beam microdiffraction and dislocations gradients, Dislocations in Solids 13 (2007) 499–601.
[43] W. Shockley, W.T. Read, Quantitative predictions from dislocation models of crystal grain boundaries, Phys. Rev. 75 (1949) 692.
[44] S.J. Lainé, K.M. Knowles, P.J. Doorbar, et al., Microstructural characterisation of metallic shot peened and laser shock peened Ti–6Al–4V, Acta Mater. 123 (2017) 350–361.
[45] A.S. Gill, A. Telang, C. Ye, et al., Localized plastic deformation and hardening in laser shock peened Inconel alloy 718SPF, Mater. Charact. 142 (2018) 15–26.
[46] L.E. Murr, J.-Y. Huang, Effect of shock-stress duration on the residual structure and hardness of nickel, chromel and Inconel, Mater Sci Eng 19 (1975) 115–122.
[47] N. Hansen, Hall-Petch relation and boundary strengthening, Scr. Mater. 51 (2004) 801–806.
[48] G.I. Taylor, The mechanism of plastic deformation of crystals. Part I.—Theoretical, Proceedings of the Royal Society of London, Series A, Containing Papers of a Mathematical and Physical Character, 145 (1934) 362–387.
[49] F.X. Kayser, C. Stassis, The elastic constants of Ni3Al at 0 and 23.5 °C, Phys Status Solidi 64 (1981) 335–342.
[50] D. Tabor, The hardness of metals, Clarendon Press, Oxford, 1951.